

Advanced numerical model for the fire behaviour of composite columns with hollow steel section

C. Renaud[†], J. M. Aribert[‡]

Laboratory of Structural Mechanics, INSA-Rennes, 35043 France

B. Zhao^{‡†}

Fire Research and Engineering Section, CTICM, 78470 St Rémy-lès-Chevreuse, France

(Received September 25, 2002, Accepted March 25, 2003)

Abstract. A numerical model is presented to simulate the mechanical behaviour of composite steel and concrete columns taking into account the interaction between the hollow steel section and the concrete core. The model, based on displacement finite element methods with an Updated Lagrangian formulation, allows for geometrical and material non linearities combined with heating over all or a part of the section and column length. Comparisons of numerical calculations made using the model with 33 fire resistance tests show that the model is able to predict the fire resistance, expressed in minutes of fire exposure, of composite columns with a good accuracy.

Keywords: composite column; hollow steel section; finite element; large displacements; slip; bond; fire situation; kinematic compatibility; plasticity; creep; iterative algorithm.

1. Introduction

During the last 30 years extensive experimental and theoretical investigations on the fire performance of unprotected steel hollow sections filled with concrete have been carried out in the World (Grimault 1980, Kordina and Klingsch 1983, Klingsch and Wittbecker 1988, Lie *et al.* 1988 to 1996). Calculation methods have been developed to predict the fire resistance of structures and structural elements. When well calibrated to experimental results such methods prove to be a practical alternative to testing structures subject to fires which is costly. In these methods the thermal and structural behaviour of composite structures under fire conditions are assumed to be uncoupled. For the purpose of the structural analysis, temperature distributions in columns are obtained separately, either from heat transfer analyse or from test data. The structural behaviour of the member is then determined in a step by step procedure using the temperature distribution provided at each time step taking into account the influence of temperature on the mechanical properties of materials.

[†]Research Assistant

[‡]Profesor and Head of Laboratory

^{‡†}Dr. Ing.

Calculation models based on the finite element method appeared on and after 1985. In these models, the mechanical behaviour of composite columns under fire condition is calculated using an incremental elasto-plastic analysis taking into account both geometrical and material non-linearities (Franssen 1987, Schleich 1987). Usually, columns are discretized by means of bar elements with two nodes and three degrees of freedom at each node. In plane bending, Bernoulli's assumption is adopted for the transversal cross-section. Effects of torsion are not considered and effects of vertical shear on the deformation energy of the element are neglected so that normal stresses are only considered. The effects of residual and thermal stresses are treated explicitly. In the presence of any temperature distribution, the longitudinal strain is given by the sum of four independent terms due to the normal stress, thermal elongation, residual stress and creep, respectively.

Alternatively, the structural stability of composite columns were calculated by a simplified method based on moment-curvature and axial strength-longitudinal strain relationship in the critical cross-section and combined with the global equilibrium equation (Quast *et al.* 1986, O'meagher *et al.* 1991, Lie *et al.* 1995, Han 2001, 2003). In such a method, the ultimate state of the column after a given duration of fire corresponds to the condition where the external bending moment in the critical cross-section exceeds the resistant moment. Successive values of the resistant moment are calculated by incrementing the longitudinal strain and the curvature (related to column deflection) and deducing the normal stresses from the stress-strain relationships of the materials. Bernoulli's assumption is adopted for the composite cross-section. This formulation takes into account explicitly the effects of differential thermal strains, geometrical imperfections and materials non-linearities on the load bearing capacity of columns. As in the methods described in (Lie *et al.* 1995, Han 2001, 2003), it may be introduced an effective buckling length for columns with end restraint which consists in modelling them as hinged at the points of contra-flexure of the member.

It should be noted that Eurocode 4 Part 1.2 provides a simplified calculation model in Annex G applicable to axially loaded circular or rectangular hollow sections (CEN 1994). For a given field of temperature, the ultimate buckling load is determined by means of a procedure similar to the one developed by Guiaux and Janss for composite hollow sections at ordinary temperature, except that the method is adapted by using temperature-dependant generalized stress-strain relationships for the steel section, reinforcement and concrete. This determination is based on the following principle: the axial buckling load at increasing temperature corresponds to the Euler critical load according to Engesser's concept of tangent modulus applied to the various materials at different temperatures (steel of hollow section, filled concrete and reinforcing steel). So an effective value of flexural stiffness for the composite column can be derived from the stress-strain relationships, assuming an equal elongation for all materials and neglecting any effect of self-equilibrated stresses due to differential thermal elongations (Grimault 1980).

In fact, all the above mentioned calculation methods to predict the fire resistance of concrete filled hollow section columns assume the full interaction between the hollow steel section and the concrete core. However, in situation of fire, this assumption proves to be inaccurate (Kordina and Klingsch 1983, Stringer and Lie 1994). As shown by measurement, the thermal elongation in the radial direction of the hollow section creates, during the fire exposure, a gap between this section and the concrete core which suggests a loss of bond leading to slip at the interface between the concrete core and the steel hollow section.

The present paper is devoted to present a novel finite element model specifically established by the authors for simulating the mechanical behaviour and resistance of both steel-concrete composite members and frames exposed to fire. In particular, this model is able to simulate more or less the interaction between the hollow steel section and the concrete core resulting in slip at the steel-concrete

interface. This is achieved by choosing the slip as an additional nodal degree of freedom. In addition to different structural configurations of columns (isolated or as a part of a frame) both geometrical and material non linearities as well as temperature distribution through the cross-sections and over the length of the columns can be taken into account.

After a presentation of the main characteristics of the model, a comparison is performed between French, German and Canadian fire test results and corresponding calculation results.

2. Presentation of the numerical model

The model presented in this paper is an advanced calculation model developed at CTICM (Zhao and Aribert 1996, 1999). In fact, this model based on the finite element method is applicable not only to steel-concrete composite columns but also to complex planar composite frames subject to any fire conditions.

2.1. Basic analytical formulation of a beam-column element in equilibrium under fire conditions

In a non-linear analysis, the equilibrium of any frame should be expressed in the updated configuration which generally requires employing an incremental formulation and introducing a time variable t , in order to describe the loading and the motion of the frame, the resolution being necessarily of iterative type to take into account the various non-linearities (geometrical and material). The formulation used in the model and the assembly of finite elements are based on the principle of virtual work expressed in an Updated Lagrangian Description; they refer to the configuration of the structure at time t to solve equilibrium problem at time $(t + \Delta t)$. In addition, it is judicious to adopt an approximate description for the local coordinates system, called “corotational”, which is commonly used in sway frames (Fig. 1).

In the model, a whole composite column is built up by means of several beam-column elements tied with connection elements. The application of the principle of virtual work for a beam-column element of homogeneous material, working in plane bending only is explained below. Effects of torsion are not

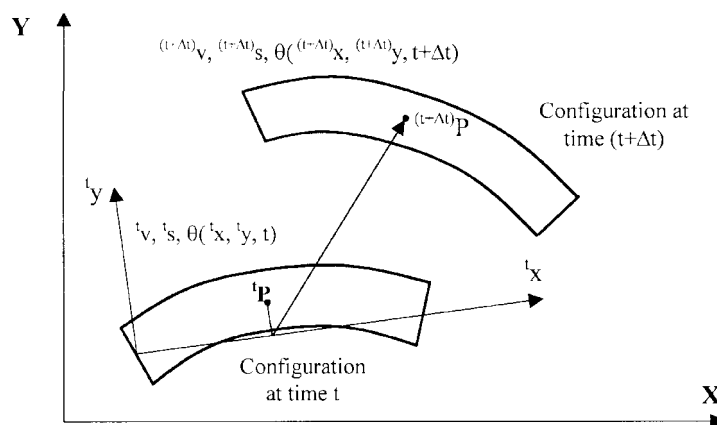


Fig. 1 Principle of updated “corotational” Lagrangian description

considered and effects of vertical shear on the deformation energy of the element have been neglected, so that the internal behaviour of the element is described by longitudinal strains and (normal) stresses at the cross-sections.

Using the “corotational” Updated Lagrangian formulation (Bathe 1982), and assuming that the strain remains small (which allows the assumption: ${}^{t+\Delta t}V = {}^tV = V$ for the volume of the element, and ${}^{t+\Delta t}S = {}^tS = S$ for its external surface), the equilibrium of any beam-column element may be expressed by the principle of virtual work as follows:

$$\int_V {}^{t+\Delta t}S_x \delta {}^{t+\Delta t}\epsilon_x dV = \int_V {}^{t+\Delta t}f_i^v \delta u_i dV + \int_S {}^{t+\Delta t}f_i^s \delta u_i dS \quad (1)$$

Here ${}^{t+\Delta t}S_x$ corresponds to 2nd Piola-Kirchoff stress tensor at time $(t + \Delta t)$ with reference to its configuration at time t ; ${}^{t+\Delta t}\epsilon_x$ corresponds to the increment of Green Lagrange strain tensor at time $(t + \Delta t)$, with reference to its configuration at time t ; ${}^{t+\Delta t}f_i^v$ et ${}^{t+\Delta t}f_i^s$ are the components of the externally applied body and surface force vectors at time $(t + \Delta t)$, with reference to its configuration at time t ; u_i is the increment of the virtual displacement vector between time t and time $(t + \Delta t)$ and δ corresponds to a virtual variation.

The normal stress and the corresponding strain can be decomposed as follows:

$${}^{t+\Delta t}S_x = {}^t\sigma_x + \Delta S_x \quad \text{and} \quad {}^{t+\Delta t}\epsilon_x = {}^t e_x + {}^t \eta_x \quad (2)$$

with

$${}^t e_x = \frac{\partial u_1}{\partial x} \quad \text{and} \quad {}^t \eta_x = \frac{1}{2} \left(\left(\frac{\partial u_1}{\partial x} \right)^2 + \left(\frac{\partial u_2}{\partial x} \right)^2 \right) \cong \frac{1}{2} \left(\frac{\partial u_2}{\partial x} \right)^2$$

where ${}^t\sigma_x$ and ΔS_x correspond to Cauchy stress tensor at time t and the increment between ${}^{t+\Delta t}S_x$ and ${}^t\sigma_x$ respectively; ${}^t e_x$ and ${}^t \eta_x$ correspond to the linear and the non-linear contribution to Green Lagrange strain tensor respectively, the above approximation for the latter being known as Von Karman hypothesis.

Linearising (from a geometrical point of view) the equilibrium equation leads to the following relation:

$$\int_V \Delta S_x \delta {}^t e_x dV + \int_V {}^t\sigma_x \delta {}^t \eta_x dV = \int_V {}^{t+\Delta t}f_i^v \delta u_i dV + \int_S {}^{t+\Delta t}f_i^s \delta u_i dS - \int_V {}^t\sigma_x \delta {}^t e_x dV \quad (3)$$

Another simplification may be introduced, which consists in neglecting second order terms to linearise the incremental behaviour as follows:

$$\Delta S_x \cong {}^t E {}^t e_x^\sigma \quad (4)$$

where ${}^t e_x^\sigma$ is the strain related to the stress increment and ${}^t E$ is the tangential modulus of the strain-stress relation defined as a function of the stress and temperature.

In addition, it should be noted that the total strain is given, in the presence of a temperature distribution in any cross-section, by the sum of four independent terms (Fig. 2), namely:

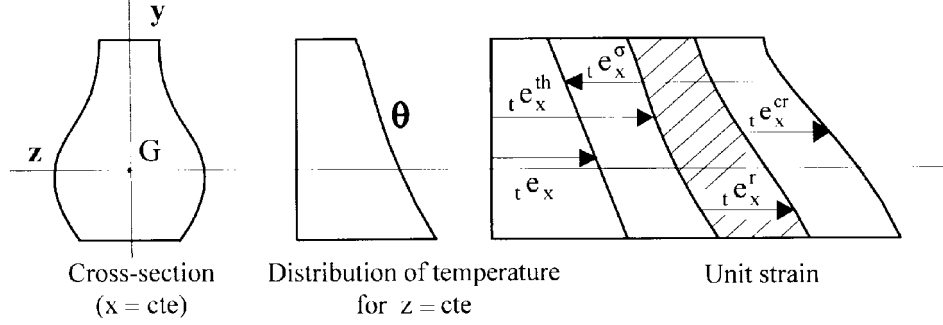


Fig. 2 Decomposition of total strain

$$\epsilon_x = \epsilon_x^\sigma + \epsilon_x^{th} + \epsilon_x^{cr} + \epsilon_x^r \quad (5)$$

where ϵ_x^{th} , ϵ_x^r and ϵ_x^{cr} are the strain increments due to thermal elongation, residual stress and creep, respectively. Obviously, the distribution of ϵ_x in each part (steel or concrete) of the cross-section must respect the Bernoulli's principle (Fig. 2).

Finally, the application of the principle of virtual work based on the incremental approach leads to the following approximate equilibrium equation:

$$\begin{aligned} & \int_V E_t \epsilon_x \delta_t \epsilon_x dV + \int_V \sigma_x \delta_t \eta_x dV \\ &= \int_V {}^{t+\Delta t} f_i^v \delta u_i dV + \int_S {}^{t+\Delta t} f_i^s \delta u_i dS - \int_V \sigma_x \delta_{t+\Delta t} \epsilon_x dV \\ &+ \int_V E(\epsilon_x^{th} + \epsilon_x^r + \epsilon_x^{cr}) \delta_t \epsilon_x dV \end{aligned} \quad (6)$$

In general, the three strain tensor increments ϵ_x^{th} , ϵ_x^r and ϵ_x^{cr} can be regarded as known quantities. This is why they have been placed in the load vector (right side of the equation).

The right part of Eq. (6) represents an “out of balance” between the virtual work of external forces at time $(t + \Delta t)$ and that of internal forces corresponding to time t . In order to reduce this “out of balance”, an iteration process should be performed, which is characterized by index k and related to the iterative increment of displacements $\Delta u_i^{(k)}$ governed by the following equation deduced from (6):

$$\begin{aligned} & \int_V E \Delta_t \epsilon_x^{(k)} \delta_t \epsilon_x dV + \int_V \sigma_x \delta \Delta_t \eta_x^{(k)} dV \\ &= \int_V {}^{t+\Delta t} f_i^v \delta u_i dV + \int_S {}^{t+\Delta t} f_i^s \delta u_i dS - \int_V \sigma_x^{(k-1)} \delta_{t+\Delta t} \epsilon_x^{(k-1)} dV \\ &+ \int_V E(\Delta_t \epsilon_x^{th(k)} + \Delta_t \epsilon_x^{r(k)} + \Delta_t \epsilon_x^{cr(k)}) \delta_t \epsilon_x dV \end{aligned} \quad (7)$$

Solving of Eq. (7) should be repeated ($k = 1, 2, 3, \dots$) until the difference between the external virtual work and the internal virtual work is negligible within a certain convergence measure (the user must

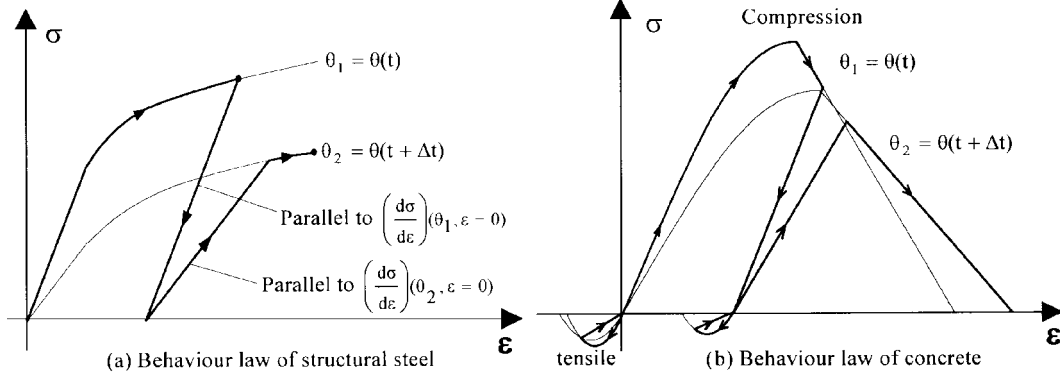


Fig. 3 Passage procedure from a behaviour curve to another

decide on the degree of accuracy required).

In fact, the repeated application of Eq. (7) corresponds to a modified Newton Raphson iteration process. The iteration is performed without updating the values of the constitutive (material property) tensor, which corresponds to adopting a constant tangent stiffness for all iterations. After the resolution of each iteration, and before starting the next iteration, all static and kinematic variables should be reinitialised as follows:

$${}^{t+\Delta t}u_i^{(k)} = {}^{t+\Delta t}u_i^{(k-1)} + \Delta u_i^{(k)}, \quad \text{with,} \quad {}^{t+\Delta t}u_i^{(0)} = {}^t u_i, \quad {}^{t+\Delta t}\sigma_i^{(0)} = {}^t \sigma_x \quad \text{and} \quad {}^{t+\Delta t}e_x^{(0)} = {}^t e_x \quad (8)$$

It should be noted that stress-strain relationships for the materials are non-linear and moreover are temperature dependant. Thus, from one temperature to another, the behaviour curve is different for the same material. The procedure adopted in the model in order to pass from a behaviour curve to another, at each step of time and thus of temperature, is schematized in Fig. 3. It consists in keeping the value of the permanent strain data from a virtual unloading at time t (also this unloading may be simplified for concrete in tension).

While in principle, the model can take into account any stress-strain relationship, the material properties recommended in Eurocode 4 Part 1.2 are generally adopted in the model. In the latter standard, creep strains of steel and concrete are considered to be implicitly included in their stress-strain relationships at elevated temperature. However when using other material properties, it is possible to introduce creep strains in the model in an explicit way. It should be noted that the procedure illustrated in Fig. 3(a) for structural steel is also considered to be applicable to the shear force-slip curve of connectors at elevated temperature deduced from experimental push-out tests (Zhao and Kruppa 1997).

As additional simplification, generally a uniform temperature is assumed over the entire column length, reducing the thermal analysis to a two-dimensional problem of transient heating through the cross-section only, which can be solved numerically using either a finite difference method (Grimault 1980, Lie and Chabot 1990, etc.) or a specialized approach such as TASEF (Wickström and Sterner 1990).

2.2. Associated matrix formulation of a homogeneous material (steel or concrete) beam-column element

The finite element used in the model to represent the steel hollow section and the concrete core is a

bar element of homogeneous material with two nodes and three degrees of freedom at each node, namely: u , v and θ defined as longitudinal displacement according to the direction ${}^i\hat{x}$, transverse displacement according to the direction ${}^i\hat{y}$, and rotation according to ${}^i\hat{z}$, respectively. The transverse displacement $v(x)$ of any point along the beam-column element is obtained assuming a cubic Hermitian shape function. Assuming also a linear interpolation in $u(x)$ and taking into account Bernoulli's assumption, the increment of displacement within an element is given by:

$$\Delta U = \begin{Bmatrix} \Delta u(x, y) \\ \Delta v(x, y) \end{Bmatrix} = [H(x, y)] \{ \Delta u_e \} \text{ with } \{ \Delta u_e \} = \{ \Delta u_i, \Delta v_i, \Delta \theta_i, \Delta u_j, \Delta v_j, \Delta \theta_j \}^T \quad (9)$$

where Δu_i , Δv_i , $\Delta \theta_i$, Δu_j , Δv_j and $\Delta \theta_j$ correspond to the nodal variables at node i and j with reference to the local coordinate system $({}^i\hat{x}, {}^i\hat{y})$, and $[H]$ correspond to the displacement interpolation matrix, as a function of x , y and L (L being the initial length of element).

The components of strain are obtained by the derivation of these displacements. They may be expressed by following relations:

$$e_x = \frac{\partial u}{\partial x} = [{}^tB_L] \{ \Delta u_e \} \text{ and } \eta_x \equiv \frac{1}{2} \left(\frac{\partial v}{\partial x} \right) = \frac{1}{2} ([{}^tB_{NL}] \{ \Delta u_e \})^2 \quad (10)$$

where the matrices $[{}^tB_L]$ and $[{}^tB_{NL}]$ are the "linear" strain matrix and the "non-linear" strain matrix, respectively, defined by:

$$[{}^tB_L] = \left\{ -\frac{1}{L}, -y \left(-\frac{6}{L^2} + \frac{12x}{L^3} \right), -y \left(-\frac{4}{L} + \frac{6x}{L^2} \right), \frac{1}{L}, -y \left(\frac{6}{L^2} - \frac{12x}{L^3} \right), -y \left(-\frac{2}{L} + \frac{6x}{L^2} \right) \right\}$$

$$[{}^tB_{NL}] = \left\{ 0, \frac{6x}{L^2} + \frac{6x^2}{L^3}, 1 - \frac{4x}{L} + \frac{3x^2}{L^2}, 0, \frac{6x}{L^2} - \frac{6x^2}{L^3}, -\frac{2x}{L} + \frac{3x^2}{L^2} \right\} \quad (11)$$

where x is the coordinate along the longitudinal axis ${}^i\hat{x}$ of the element.

It should be noted again that the non-linear strain matrix is only related to the contribution of transverse displacement v and the influence $(\partial u / \partial x)^2$ is neglected owing to the fact that the axial deformation remains in general relatively small.

Introducing relations (9) to (11) into the iteration equilibrium Eq. (7), the following matrix formulation can be obtained:

$$([{}^tK_{eL}] + [{}^tK_{eNL}]) \{ \Delta u_e^{(k)} \} = \{ {}^{t+\Delta t}R_e \} - \{ {}^{t+\Delta t}F_e^{(k-1)} \} + \{ \Delta_t F_{e\ th, cr, r}^{(k)} \} \quad (12)$$

where:

- $[{}^tK_{eL}]$ and $[{}^tK_{eNL}]$ are tangential stiffness matrices corresponding respectively to the linear strain part and the non-linear strain part (in direct relation with the change of geometry):

$$[{}^tK_{eL}] = \int_{V_e} [{}^tB_L]^T {}^tE [{}^tB_L] dV \text{ and } [{}^tK_{eNL}] = \frac{1}{2} \int_{V_e} [{}^tB_{NL}]^T {}^t\sigma_x [{}^tB_{NL}] dV \quad (13)$$

leading to following total stiffness matrix of the beam-column element:

$$[{}^tK_e] = [{}^tK_{eL}] + [{}^tK_{eNL}] \quad (14)$$

whose dimension is 6×6 .

- $\{{}^{t+\Delta t}R_e\}$ is the vector of nodal external forces at time $(t + \Delta t)$:

$$\{{}^{t+\Delta t}R_e\} = \int_{V_e} [H]^T \{{}^{t+\Delta t}f_V\} dV + \int_{S_e} [H]^T \{{}^{t+\Delta t}f_S\} dS \quad (15)$$

- $\{{}^{t+\Delta t}F_e^{(k-1)}\}$ is a vector of equivalent nodal forces resulting from the work of internal forces due to the change of configuration (including the internal forces of the discretised shear connection), corresponding to time $(t + \Delta t)$ and iteration $(k-1)$:

$$\{{}^{t+\Delta t}F_e^{(k-1)}\} = \int_{V_e} [{}^tB_L]^T {}^{t+\Delta t}\sigma_x^{(k-1)} dV \quad (16)$$

- $\{\Delta_t F_e^{(k)}\}_{th, cr, r}$ is also a vector of equivalent nodal forces due to the strain increases resulting from thermal elongation and creep and due to possible residual stresses in the materials:

$$\{\Delta_t F_e^{(k)}\}_{th, cr, r} = \int_{V_e} [{}^tB_L]^T E (\Delta_t e_x^{th(k)} + \Delta_t e_x^{cr(k)} + \Delta_t e_x^{r(k)}) dV \quad (17)$$

2.3. Matrix formulation of a steel-concrete composite beam-column element

2.3.1. Vector of nodal displacement (in a generalised global coordinate system)

Any composite column whose flexural bending occurs in a symmetrical plane may be idealised as an assemblage of three specific finite elements (Fig. 4), namely:

- a first beam-column element for a certain length of steel hollow section (superscript (a)) with a node at each end and three degrees of freedom (two translations and one rotation) at each node;
- a second beam-column element for concrete core (superscript (b)) corresponding to the same initial length as the steel element and having also two nodes;
- and a connection element with two nodes and only one degree of freedom per node corresponding to the discretisation of the distributed shear connection between the steel and concrete beam-column elements.

Bernoulli's assumption is adopted for the cross-section of the above-mentioned bar elements and any gap phenomenon between hollow steel section and concrete core is neglected so that the unknown variables at node i used to solve the global equilibrium problem can be reduced to:

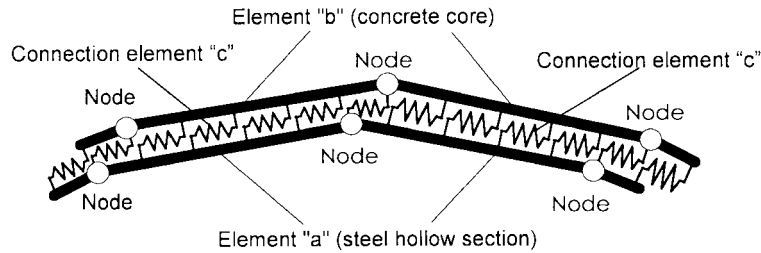


Fig. 4 Specific composite bar element

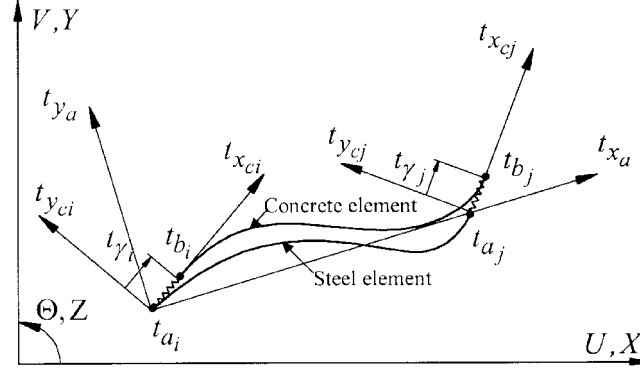


Fig. 5 Nodal, local and global coordinate systems

$$\{\Delta D_i\} = [\Delta u_i^{(a)}, \Delta v_i^{(a)}, \Delta \theta_i^{(a)}, \Delta \gamma_i]^T \quad (18)$$

where:

- $\Delta u_i^{(a)}, \Delta v_i^{(a)}, \Delta \theta_i^{(a)}$ are the increments, between t and $(t + \Delta t)$, of the usual nodal variables referred to the global coordinate system of the column and related to the translational displacement in \vec{X} direction, the translational displacement in \vec{Y} direction and the rotation around \vec{Z} axis, respectively.
- $\Delta \gamma_i$ is a nodal variable which corresponds to the increment of relative displacement between the steel and concrete parts, at node i in the tangential direction to the interface in the configuration at time t . In fact $\Delta \gamma_i$ is a slip increment according to a familiar meaning.

Consequently, the variables are referred to in a generalised global coordinate system needing a further treatment to establish the iteration equilibrium matrix equation of the whole composite element. Fig. 5 illustrates the different coordinate systems which are used in the model.

2.3.2. Connection finite element between steel and concrete

The connection element developed to link both beam-column elements permits expressing full, partial or zero shear connection (mechanical bond) at the steel-concrete interface. The thickness of this element is taken equal to zero, and its material matrix relates the bond stresses along the steel-concrete interface to the relative displacements between concrete and steel, namely the slip.

Using the assumption of a linear shape function, the increment of slip at each point of the element is related to the increments of nodal slip $\Delta \gamma_i$ and $\Delta \gamma_j$ as follows:

$$\Delta \gamma(s) = [N(s)] \begin{Bmatrix} \Delta \gamma_i \\ \Delta \gamma_j \end{Bmatrix} \quad (19)$$

$N(s)$ is the displacement interpolation matrix defined by: $[N(s)] = \left[1 - \frac{s}{\widehat{\mathcal{L}}_{ij}}, \frac{s}{\widehat{\mathcal{L}}_{ij}} \right]$ where s corresponds to the curvilinear coordinate along the connection element and $\widehat{\mathcal{L}}_{ij}$ is the adapted length of this element corresponding to the curvature of neutral fibre of steel bar element, assembled with the connection element. Then, the tangential stiffness matrix of the connection element, whose dimension is 2×2 , is given by:

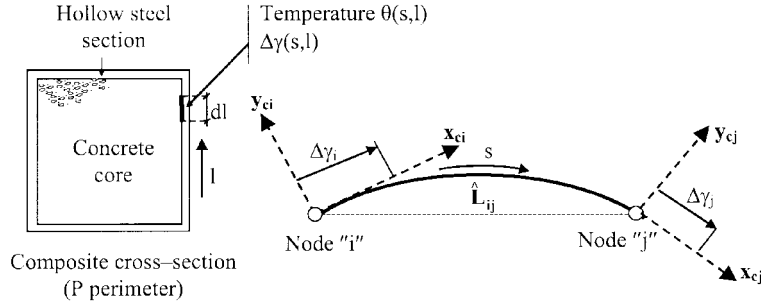


Fig. 6 Two nodes connection element

$$[{}^tK_{ec}] = \int_P \int_{L_{ij}} [N(s)]^T k_c(s, l) [N(s)] dl ds \quad (20)$$

where coefficient $k_c(s, l)$ is the tangential modulus of the “shear stress-slip” curve characterising mechanical bond at the steel-concrete interface for temperature $\theta(s, l)$ at time t ; P is the perimeter of the steel-concrete interface at the cross-section considered and l is the curvilinear coordinate along the perimeter.

To evaluate the element stiffness and the nodal equivalent forces resulting from the stresses in the elements, integration over the element volume should be applied. In case of a homogeneous elastic behaviour, this can be performed in an analytical way. However it is no longer possible when fibres of the element have an inelastic behaviour. Consequently, a numerical procedure using certain representative integration points along the element is adopted. At each point, the corresponding element section is discretized by means of numerous sub-sections to represent suitably the section geometry and to take into account both the variation of temperature and the non-linear behaviour of fibres. Concerning the connection element, the numerical integration of the stiffness matrix over the steel-concrete interface is based on a two point Gauss quadrature formula, discretizing the perimeter by means of segments dl (Fig. 6). A similar procedure was adopted for the bar elements.

2.3.3 Transformation of the element stiffness matrix into the generalised global system

a) Steel and concrete beam-column element

For the usual 2D bar elements, the vector of nodal displacements contains six variables. The stiffness matrix of each element can be established easily in the ordinary global coordinate system X, Y, Z . But concerning the specific composite bar element developed in the model, height variables are necessary. These variables, not defined in the same coordinate system, need to be transformed so that the stiffness matrix of the two bar elements constituting the steel-concrete composite element can be expressed in the generalised global coordinate system.

Considering the tangential stiffness matrix of the concrete element, $[{}^t k_e^{(b)}]$ (as defined in Eq. (14)), determined at time t and referred to the configuration also at time t characterized by the local coordinate system (\vec{x}_b, \vec{y}_b) , it is easy to express the stiffness matrix in the global coordinate system by the following transformation:

$$[{}^t K_e^{(b)}] = \begin{bmatrix} T_b & 0 \\ 0 & T_b \end{bmatrix}^T [{}^t k_e^{(b)}] \begin{bmatrix} T_b & 0 \\ 0 & T_b \end{bmatrix} \quad (21)$$

where $[T_b]$ is the rotation matrix, with dimension 3×3 , allowing a transformation from the local

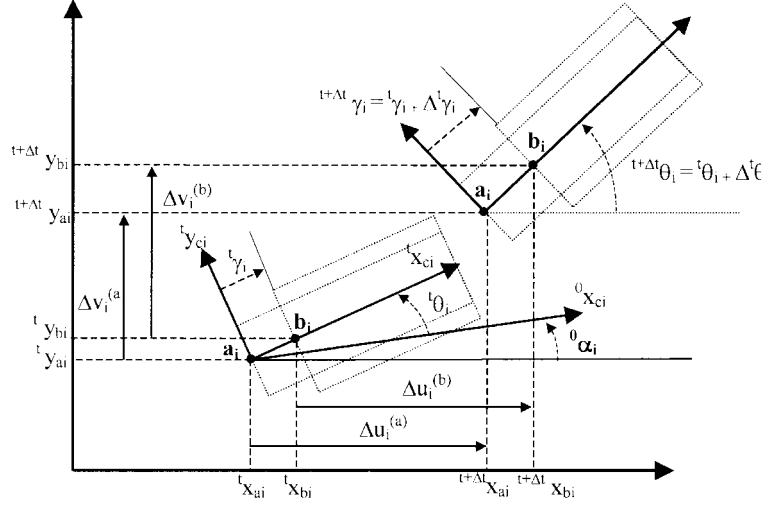


Fig. 7 Kinematic compatibility between increments of displacements, rotations and slip at node i

system $(\vec{x}_b, \vec{y}_b, \vec{z})$ to the global one $(\vec{X}, \vec{Y}, \vec{Z})$.

To transfer to the generalised global system, the nodal variables may be replaced by the variables mentioned in Eq. (18) for node i and the similar ones for node j . At node i , a certain kinematic compatibility between all variables should be satisfied when the composite element moves from the configuration at time t to the configuration at time $(t + \Delta t)$. Let θ_i be the total rotation of node i at time t , and ${}^0\alpha_i$ the initial angle between the nodal axis used to define the slip variable and the global axis. The following relationship of kinematic compatibility for the concrete element at node i can be established:

$$[\Delta u_i^{(b)}, \Delta v_i^{(b)}, \Delta \theta_i]^T = [\tilde{T}_{bi}][\Delta u_i^{(a)}, \Delta v_i^{(a)}, \Delta \theta_i, \Delta \gamma_i]^T \quad (22)$$

where:

$$[\tilde{T}_{bi}] = \begin{bmatrix} 1 & 0 & -\gamma_i \cdot \sin[\theta_i + {}^0\alpha_i] & \cos(\theta_i + {}^0\alpha_i) \\ 0 & 1 & \gamma_i \cdot \cos(\theta_i + {}^0\alpha_i) & \sin(\theta_i + {}^0\alpha_i) \\ 0 & 0 & 1 & 0 \end{bmatrix} \quad (23)$$

Then the stiffness matrix $[\tilde{K}_e^{(b)}]$ of the concrete element in the generalized global coordinate system can be derived from following relation:

$$[\tilde{K}_e^{(b)}] = \begin{bmatrix} \tilde{T}_{bi} & 0 \\ 0 & \tilde{T}_{bj} \end{bmatrix}^T [\tilde{K}_e^{(b)}] \begin{bmatrix} \tilde{T}_{bi} & 0 \\ 0 & \tilde{T}_{bj} \end{bmatrix} \quad (24)$$

where \tilde{T}_{bj} is similar to (23), but for node j .

It should be noted that the elementary stiffness matrix has a dimension of 6×6 , whereas the transformed matrix has now a dimension of 8×8 .

The stiffness matrix $[\tilde{K}_e^{(a)}]$ of the steel element can be constructed according to a similar procedure as above while noting that the matrices \tilde{T}_{ai} and \tilde{T}_{aj} , allowing a transformation to the generalised global system, are very simple:

$$[\tilde{T}_{ai}] = [\tilde{T}_{aj}] = \begin{bmatrix} 1 & 0 & 0 & 0 \\ 0 & 1 & 0 & 0 \\ 0 & 0 & 1 & 0 \\ 0 & 0 & 0 & 0 \end{bmatrix} \quad (25)$$

b) Connection element

As for the connection element for node i and j , its tangential stiffness matrix may be easily determined in the generalized global system due to the choice of the end slips as nodal variable. It can be obtained by:

$$[{}^t\tilde{K}_{ec}] = \begin{bmatrix} T_c & 0 \\ 0 & T_c \end{bmatrix}^T [{}^tK_{ec}] \begin{bmatrix} T_c & 0 \\ 0 & T_c \end{bmatrix} \quad \text{where: } [T_c] = [0 \ 0 \ 0 \ 1] \quad (26)$$

and $[{}^tK_{ec}]$ has been defined in relationship (20).

At the present stage, the tangential stiffness matrix of the connected composite element, $[{}^t\tilde{K}_e]$, can be deduced using a direct algorithm of summation of the elementary matrices $[{}^t\tilde{K}_e^{(a)}]$, $[{}^t\tilde{K}_e^{(b)}]$, and $[{}^t\tilde{K}_{ec}]$.

2.4. Transformation of the load vector into the generalised global system

In consistence with the type of composite finite element developed here, the loading vector R_i at node i needs to make a distinction between two sub-vectors R_{ai} and R_{bi} among the external forces and the moment applied to the node since the steel and concrete parts have different displacements.

Defining the steel part and the concrete part of loading at node i in the ordinary global system as:

$$\{{}^{t+\Delta t}R_{ai}\} = [{}^{t+\Delta t}F_{ai}, {}^{t+\Delta t}P_{ai}, {}^{t+\Delta t}M_{ai}]^T \quad \text{and} \quad \{{}^{t+\Delta t}R_{bi}\} = [{}^{t+\Delta t}F_{bi}, {}^{t+\Delta t}P_{bi}, {}^{t+\Delta t}M_{bi}]^T \quad (27)$$

where F , P and M correspond to the components of two forces and one moment, respectively.

Multiplying on the left $\{{}^{t+\Delta t}R_{ai}\}$ and $\{{}^{t+\Delta t}R_{bi}\}$ by the corresponding transposed transformation matrices, namely matrices $[\tilde{T}_{ai}]^T$ and $[\tilde{T}_{bi}]^T$, we obtain in the generalised global system the two new following loading vectors:

$$\{{}^{t+\Delta t}\tilde{R}_{ai}\} = [{}^{t+\Delta t}F_{ai}, {}^{t+\Delta t}P_{ai}, {}^{t+\Delta t}M_{ai}, 0]^T \quad (28)$$

and

$$\{{}^{t+\Delta t}\tilde{R}_{bi}\} = \left\{ \begin{array}{c} {}^{t+\Delta t}F_{bi} \\ {}^{t+\Delta t}P_{bi} \\ {}^{t+\Delta t}M_{bi} - \sin({}^t\theta_i + {}^0\alpha_i) {}^t\gamma_i \cdot {}^{t+\Delta t}F_{bi} + \cos({}^t\theta_i + {}^0\alpha_i) {}^t\gamma_i \cdot {}^{t+\Delta t}P_{bi} \\ \cos({}^t\theta_i + {}^0\alpha_i) {}^{t+\Delta t}F_{bi} + \sin({}^t\theta_i + {}^0\alpha_i) {}^{t+\Delta t}P_{bi} \end{array} \right\} \quad (29)$$

Then regrouping the above two loading sub-vectors leads to the following final loading vector at node i in the generalised global system:

$$\{ {}^{t+\Delta t} \tilde{R}_i \} = \left\{ \begin{array}{c} {}^{t+\Delta t} F_{ai} + {}^{t+\Delta t} F_{bi} \\ {}^{t+\Delta t} P_{ai} + {}^{t+\Delta t} P_{bi} \\ {}^{t+\Delta t} M_{ai} + {}^{t+\Delta t} M_{bi} - \sin({}^t \theta_i + {}^0 \alpha_i) {}^t \gamma_i \cdot {}^{t+\Delta t} F_{bi} + \cos({}^t \theta_i + {}^0 \alpha_i) {}^t \gamma_i \cdot {}^{t+\Delta t} P_{bi} \\ \cos({}^t \theta_i + {}^0 \alpha_i) {}^{t+\Delta t} F_{bi} + \sin({}^t \theta_i + {}^0 \alpha_i) {}^{t+\Delta t} P_{bi} \end{array} \right\} \quad (30)$$

As an interpretation, the sub-vector $[{}^{t+\Delta t} F_{ai} + {}^{t+\Delta t} F_{bi}, {}^{t+\Delta t} P_{ai} + {}^{t+\Delta t} P_{bi}, {}^{t+\Delta t} M_{ai} + {}^{t+\Delta t} M_{bi}]^T$ corresponds to the external loads accumulated for the materials “a” and “b” and associated only with the increases in nodal displacements $\Delta u_i, \Delta v_i, \Delta \theta_i$. This sub-vector is completed at the third and the fourth lines of Eq. (30) by contributions coming from the external loads related to material b through the effect of the nodal variable (that is slip) $\Delta \gamma_i$.

2.5. Solving of the global equilibrium equation

After assembling the various composite bar elements and taking into account the boundary conditions, the global equilibrium matrix equation of the structure can be expressed in the following incremental form:

$$[{}^t \tilde{K}] \{ \Delta D^{(k)} \} = \{ {}^{t+\Delta t} \tilde{S} \} - \{ {}^{t+\Delta t} F_G^{(k-1)} \} + \{ \Delta_t F_{th, cr, r}^{(k)} \} \quad (31)$$

and is associated with a Newton Raphson iteration process for resolution. It is clear that Eq. (31) has the same appearance as the elementary Eq. (12), but now with the following symbols:

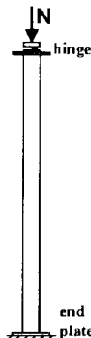
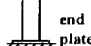
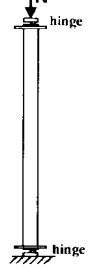
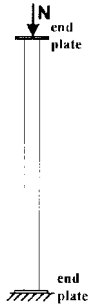
- $[{}^t \tilde{K}]$ is the tangential stiffness global matrix of the structure;
- $\{ \Delta D^{(k)} \}$ is the incremental vector of the generalised nodal displacements at iteration (k) ;
- $\{ {}^{t+\Delta t} \tilde{S} \}$ is the vector of the nodal external forces at time $(t + \Delta t)$;
- $\{ {}^{t+\Delta t} F_G^{(k-1)} \}$ is a vector of equivalent nodal forces resulting from the work of internal forces due to the change of configuration (including the internal forces of the discretised connection), corresponding to time $(t + \Delta t)$ and iteration $(k-1)$;
- $\{ \Delta_t F_{th, cr, r}^{(k)} \}$ is also a vector of equivalent nodal forces due to the strain increases between t and $(t + \Delta t)$ resulting from thermal elongation (subscript th), creep (subscript cr) and possible residual stresses (subscript r) in the materials.

Once equation (31) is solved, the displacements should be updated as follows:

$$\{ {}^{t+\Delta t} D^{(k)} \} = \{ {}^{t+\Delta t} D^{(k-1)} \} + \{ \Delta D^{(k)} \} \quad (32)$$

Adopting $\{ {}^{t+\Delta t} D^{(0)} \} = \{ {}^t D \}$ in relationship (32), the iteration process is performed for $k = 1, 2, 3, \dots$, until the “out-of-balance” in Eq. (31) is negligible within a certain convergence measure.

Table 1 Structural properties and failure times of tested columns

Test	Profile type	Rebars	Length (mm)	End conditions	Test loading		Material properties(N/mm ²)			Measured failure time (min)	Maximum temperature in steel (°C)
					Load (KN)	Eccentricity(mm)	Steel	Rebars	Concrete		
1	200×6.3	4φ18	4200		432	20	277	475	45.9	63	975
2	200×6.3	4φ18	4200		318	50	277	475	45.9	58	950
3	200×6.3	4φ18	4200		537	5	291	475	42.9	61	950
4	200×6.3	4φ18	3700		649	20	300	475	55	39	880
5	200×6.3	-	4200		400	20	279	-	55	22	750
6	200×6.3	4φ18	3700		649	20	265	475	75	56	1010
7	200×6.3	4φ18	4200		550	5	274	475	75	59	1035
8	200×6.3	4φ18	3700		294	20	281	469	35	82	1100
9	200×6.3	4φ18	4200		375	22	287	469	35	68	920
10	200×12.5	4φ18	4200		453	50	234	475	45.9	34	775
11	300×7.0	4φ14	3621		1500	50	327	441	38	57.3	780
12	300×7.0	4φ14	3619		1500	100	327	441	38	25	600
13	150×5.0	4φ12	3810		140	0	416	596	37.8	82	1010
14	200×5.0	8φ10	3600		500	7	378	494	38.5	62	830
15	200×5.0	4φ10	3600		500	15	378	494	38.5	56.4	830
16	200×5.0	4φ6	3490		1000	0	598	500	32.5	23	600
17	200×10.0	4φ6	3430		1200	5	598	500	36.5	27.1	600
18	273.1×6.35	4φ20	3810		1050	0	350	400	46.7	188	1050
19	273.1×6.35	4φ20	3810		1900	0	350	400	47.0	96	930
20	300×7.0	8φ20	3600		1870	0	331	441	32.5	136	1030
21	300×7.0	8φ20	3600		2570	0	331	441	32.5	59	840
22	300×8.0	4φ32	3810		1400	66	394	596	43.8	58	920
23	168.3×4.8	-	3810		150	0	350	-	32.7	76	910
24	168.3×4.8	-	3810		150	0	350	-	35.4	81	930
25	203×6.35	4φ16	3810		930	0	350	400	48.1	105	845
26	219.1×4.78	-	3810		492	0	350	-	31.0	80	925
27	219.1×4.78	-	3810		384	0	350	-	32.3	102	960
28	254×6.35	4φ20	3810		1440	0	350	400	48.1	113	990
29	254×6.35	4φ20	3810		2200	0	350	400	48.1	70	880
30	273.1×5.56	-	3810		574	0	350	-	28.6	112	955
31	273.1×5.56	-	3810		525	0	350	-	29.0	133	985
32	273.1×5.56	-	3810		574	0	350	-	27.2	70	860
33	355.6×12.7	-	3810		1050	0	350	-	25.4	170	1030

More detailed developments on the above topic can be found in references (Zhao and Aribert 1996, 1999, Renaud, Aribert, Zhao, and Grimault 2000, Renaud, Aribert, and Zhao 2002).

3. Comparaison of the model with fire tests

Thirty-three fire tests are considered here which were carried out in France (Fire station of CTICM in “Maizières-Les-Metz”), in Germany (University of Braunschweig) supported by CIDECT research projects (Cidect 1983) and in Canada (Institute for Research in Construction, National Research Council of Canada).

3.1. Test conditions

The main structural properties of every column and its experimental failure time are summarised in Table 1.

In a standard fire test, the column, located at the centre of a furnace, is subjected to a constant axial load up to the failure, while being exposed to heating controlled in such a way that the average temperature in the furnace follows, as closely as possible, the “standard time-temperature curve” (ISO curve). Some of the columns tested had both ends hinged (rocker bearings), while others had a hinge at one end and an end plate at the other end. Most of the columns were tested under an eccentric load.

During all the tests, the furnace temperature was continuously recorded. Thermocouples were installed on the hollow section and the reinforcing bars as well as in the concrete core. In fact, three cross-sections were equipped along the column length in order to measure the temperature field. The axial displacement at the top of the column and the transverse column deflection at mid-height (only for German tests) were systematically recorded during the tests. Except for most of Canadian tests, specimens from the steel sections, reinforcing bars and concrete were used to obtain the actual mechanical properties (yield and ultimate tensile strengths of steel and compressive strength of concrete).

3.2. Assumptions for numerical simulations

In addition to the loading, boundary and heating conditions described in the previous paragraph, the model needs to adopt other physical assumptions to compensate inevitable uncertainties in fire tests, as follows:

- The thermal and mechanical materials properties as a function of temperature were taken to be in accordance with EC4 Part 1.2 (1994). It may be underlined that the creep strains of steel and concrete are implicitly included in the stress-strain relationships at elevated temperature.
- Over the height of the column a uniform temperature has been assumed for the German tests. With regard to the French tests, a temperature gradient at the top of the columns has been taken into account over about thirty centimetres. This temperature gradient was due to the fact that the top of the column, being outside the furnace during the test, was not heated directly by fire but by conduction.
- All the columns were tested without measuring their out-of-straightness. An out-of-straightness of $L/500$ was however used in the numerical simulations (tolerance given by the manufacturer). It was considered to be always on the side leading to a cumulative effect with the loading eccentricity.
- In each column, the effect of slip between the concrete core and the steel wall was assumed to occur without significant bond between steel and concrete.

3.3. Presentation of two simulations

To illustrate the effects of end restraint conditions of columns and of slip at the steel-concrete interface, the behaviour of test number 1 and test number 13 (see Table 1) are simulated with or without slip and with two different end conditions (namely hinged at both ends or fixed at one end and hinged at the other end).

For test number 1, the temperature measurements obtained at several points of the section has allowed introducing a temperature field of sufficient accuracy directly into the numerical simulation. For test number 13, temperature distributions have been computed using a numerical model based on the finite difference method (which was proved to simulate the thermal behaviour of composite

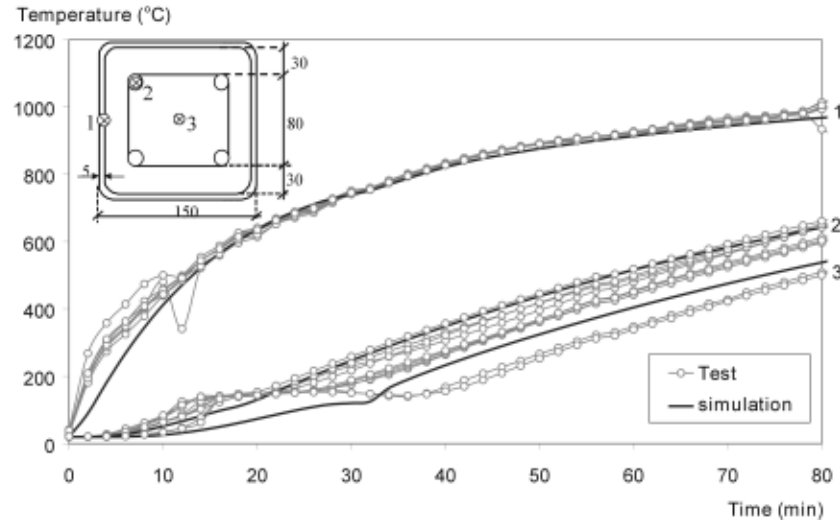


Fig. 8 Calculated and measured temperatures in the column cross-section of test number 13

columns appropriately and to provide a good estimation of the temperature field (Grimault 1980). In this model, non-linearities due to the temperature dependence of materials properties and boundaries conditions are taken into account. It is assumed that conduction is the main heat transfer mechanism in the hollow steel section and concrete core. Convection and radiation act essentially for heat transfers from fire to the hollow steel section. The influence of moisture (assumed uniformly distributed in the concrete) is treated in a simplified way: the transient temperatures in the concrete cross-section are calculated assuming that all moisture evaporates, without any transfer, at the temperature 100°C (or at another temperature within a narrow range with the heat of evaporation giving a corresponding change in the enthalpy-temperature curve). So, during the period of evaporation, all the heat supplied to an element is used for the moisture evaporation until the element is dry.

For test number 13, the calculated temperatures are compared to the measured ones at the hollow steel section and at various points of the concrete core (including reinforcement) in Fig. 8.

In the hollow steel section the calculated temperatures are in good agreement with the measured ones. The temperatures in the longitudinal reinforcement are simulated satisfactorily between 0 and 100°C . However, measured temperatures rise more rapidly than calculated temperatures during this period, because of important vapour diffusion of hot layers of concrete towards cold layers. Once the temperature of 100°C is reached close to the reinforcement, calculated temperatures becomes appreciably more important than those measured (the maximum difference is about 100°C). Globally, the predicted curve of temperature rise is analogous with those observed in experiments, but somewhat translated towards lower times (the translation between the curves corresponds to the time necessary to the vaporisation of water contained in the concrete). Differences between calculations and tests are explained on the one hand by a certain uncertainty of real moisture content (fixed at 4% in calculations) and on the other hand by a water accumulation close to the reinforcement subsequent to water migration (not taken into account in the model). In fact, one part of this water escapes by cracks towards the hollow section, while the other part migrates towards the coldest zones where it condenses again, which result in a slowing down of the vaporisation phase and consequently increases the length of the vaporisation stage. With regard to the point inside the concrete, the agreement is not so good, but

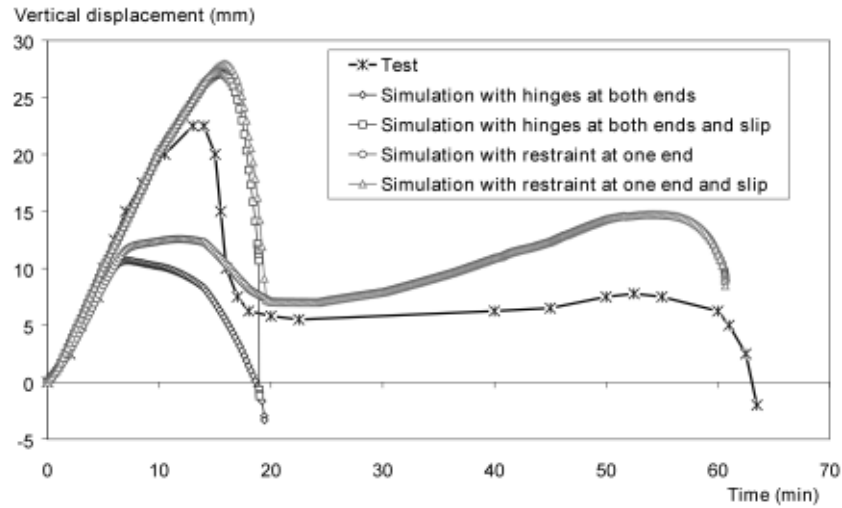


Fig. 9 Vertical displacement at the column top of test number 1

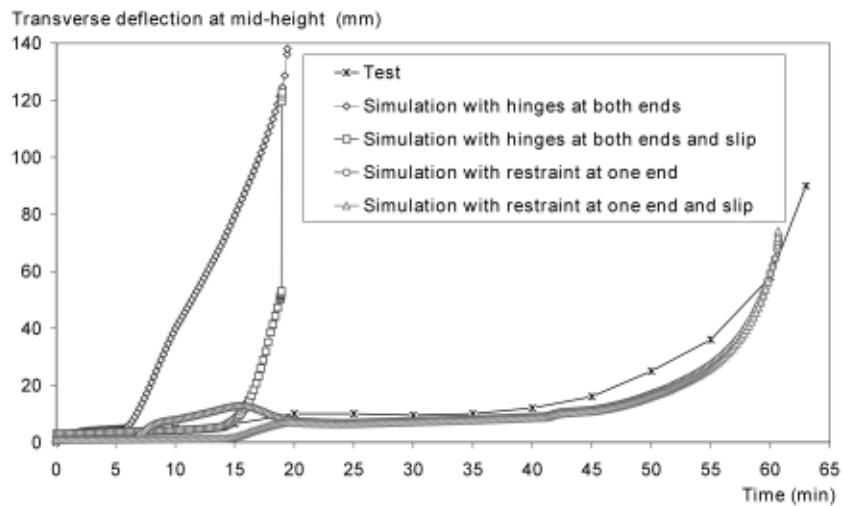


Fig. 10 Transverse deflection at mid-height of column of test number 1

can nevertheless be regarded as satisfactory. Difference between theoretical and experimental curves is without too significant consequences: for low temperatures, the concrete mechanical are not affected and for higher temperatures the calculated curve is on the safe side.

At room temperature, these columns were designed as hinged at both ends. Assuming the same support conditions during the fire, the calculated failure time of the column number 1 is 19 minutes, which is very far from the test failure time (63 minutes). As for test number 13, it is 17 minutes for a measured value of 82 minutes. In reality, observation of the bending deflection of the column after the test has suggested trying others support conditions, namely a hinged support at one end and a restraint condition at the other end. Using these new support conditions, the failure time becomes 61 minutes for columns number 1, and 77 minutes for column number 13, which now is close to the measured time.

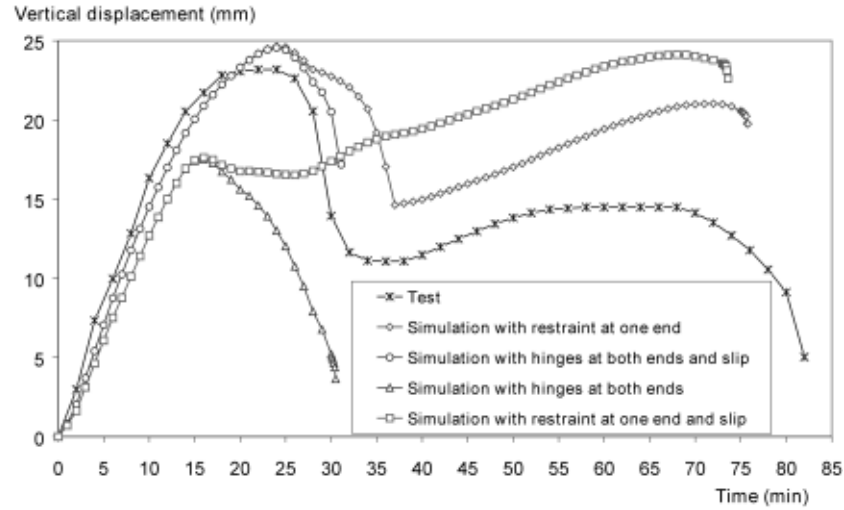


Fig. 11 Vertical displacement at mid-height of column of test number 13

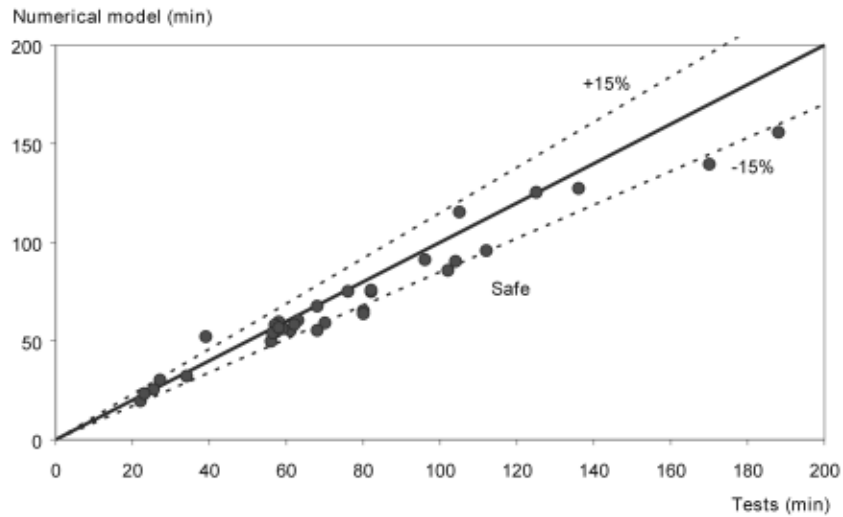


Fig. 12 Comparison of fire resistances between the numerical model and tests

Generally, individual columns with either end plates or bearings at the top and bottom are both assumed to provide hinged supports (see end details in Table 1). As an explanation as to why the above result appears to prove otherwise, it is presumed that additional restraints may result from the parts of the structure only partially affected by the fire temperature above and below the column ends and therefore having a higher stiffness.

The evolution of the vertical displacement calculated at the top of the column number 1 and of the transverse deflection calculated at mid-height of the column is shown in Fig. 9 and Fig. 10, respectively. These displacements are compared to the measured ones. Fig. 11 present the vertical displacement calculated at the top of the column number 13. The transverse deflection at mid-

Table 2 Failure time of columns simulated with or without slip

Test	1	2	3	4	5	6	7	8	9	10	11	12	13	14	15	16	17	
Calculated failure time	Without slip	60.7	55.4	55.5	50.2	18.8	55.4	59.1	77.2	61.4	32.4	54.7	27.1	75.6	60.8	53.7	23.5	302
	With slip	60.8	58.4	55.3	50.0	21.3	55.5	59.5	79.4	63.5	32.9	55.6	25.6	75.8	60.6	54.7	23.4	30.0
Test	18	19	20	21	22	23	24	25	26	27	28	29	30	31	32	33		
Calculated failure time	Without slip	155.6	91.8	125.8	58.1	57.7	78.2	63.8	90.6	67.4	88.8	97.8	59.6	118.0	128.2	56.3	142.6	
	With slip	155.8	91.2	124.8	58.2	57.2	75.2	67.2	90.4	65.4	85.8	97.4	59.2	115.4	125.4	55.4	139.6	

height has not been the subject of measurement during this test, so that no comparison with the model is possible.

In the case of restraint conditions (fixed) at the one end, there is a good agreement between measured and calculated displacements, in particular when the slip is taken into account. Whereas the transverse deflection calculated at mid-height is practically the same as the one measured, it should be noted that column elongation is somewhat over-estimated near the end of the test. A possible explanation of this difference may be the fact that the column is not uniformly overheated over its whole length.

In addition, the fact of introducing into the simulations the temperatures directly measured at some cross-section points may involve an over-estimate of unknown temperatures inside the concrete, and consequently lead to overestimating thermal dilation. It should be noted that a difference exists again in the neighbourhood of the fifteenth minutes, which may be explained by certain bond persistence between the steel tube and the concrete core, in spite of the important rise of temperature.

Except during the first 30 minute, the slip does not seem to have a significant influence on the column deformation, and consequently on the time of fire stability.

3.4. Synthesis of results

Calculations have been performed dealing with the 33 column tests carried out in France, Germany and Canada. Globally the difference between failure times ascertained numerically and experimentally does not exceed 15% as illustrated in Fig. 12, which is fully acceptable considering the various uncertainties inherent to test data, such as the heating condition along the height column, the degree of rotational restraint at the column ends, the unintentional eccentricity of axial load, the initial out-of-straightness of the column, etc.

The good agreement of the model in comparison with tests is due not only to the choice of appropriate material laws as well as introduction of column imperfections (initial out-of-straightness, residual stresses) but also to the ability to take into account the phenomenon of slip between the steel tube and the concrete core.

All the numerical results confirm that the slip has no significant influence on the failure time of composite columns, provided that the hollow section is filled with reinforced concrete. However it leads to a more realistic evolution path of the displacements (vertical displacement and deflection) during the first period of heating as already shown in Figs. 9 to 11. On the contrary, columns without reinforcement and columns subject to important bending moments appear to be more sensitive to the phenomenon of slip which may influence not only their deformations but also their failure time (see Table 2).

4. Conclusions

The main features of a finite element model specifically implemented by the authors to analyse the fire resistance of composite structures taking into account the effect of the interface slip between steel and concrete have been presented. Using this model, the fire resistances of several composite columns with concrete filled hollow sections have been calculated and compared with test results. These comparisons show that the model can simulate appropriately the structural behaviour of composite columns and provide a good estimation of the fire resistance time.

A simplified semi-analytical method to evaluate the fire resistance of columns composed of unprotected concrete filled hollow sections is available in Annex G of Eurocode 4 (ENV 1994-1-2). Several research works related to this method have demonstrated its questionable level of approximation with regard to buckling resistance predictions at elevated temperatures, in particular the method leads to a safety level that depends clearly on the slenderness of the columns, being unsafe for intermediate slendernesses (Twilt and Haar 1984, 1985). In the near future, the model will be used to perform a very wide series of numerical simulations for many values of significant parameters affecting the performance of composite columns such as buckling length, fire duration, cross-section size, and considering the standard fire exposure. Referring to this base of numerical results, it may be expected that a more suitable simplified method will be established, taking into account globally the effects of restrained thermal stresses and initial deflection of the columns on the load bearing capacity of columns. These effects are entirely neglected in Annex G but they may become important for columns with high buckling lengths. Another aim of the work will consist in using the same type of buckling approach proposed at room temperatures given in Eurocode 4, but modifying material properties at elevated temperatures.

References

- Aribert, J.M. and Zhao, B. (1999), "Analysis of the fire behaviour of composite steel-concrete structures", *French Journal of Steel Construction*, n°3, 37-48.
- Bathe, K.J. (1982), *Finite Element Procedures in Engineering Analysis*, Prentice Hall Civil Engineering.
- CEN, Eurocode 4-Part1.2 (ENV) (1994), "Design of composite steel and concrete structures: structural fire design".
- Franssen, J.M. (1987), "Etude du comportement au feu des structures mixtes acier-béton", Thèse de Doctorat, université de Liège.
- Grimault, J.P. (1980) "Détermination de la durée au feu des profils creux remplis de béton", Rapport final établi par Cometube, Commission des Communautés Européennes, Recherche Technique Acier, Paris.
- Han, L.H. (2001). "Fire performance of concrete filled steel tubular beam-columns", *Journal of Constructional Steel Research*, **57**(6), 697-711.
- Han, L.H., Yang, Y.F. and Xu, L. (2003a). "An experimental study and calculation of the fire resistance of concrete-filled hollow steel columns", *Journal of Constructional Steel Research*, **59**(4), 427-452.
- Han, L.H., Zhao, X.L., Yang, Y.F. and Feng, J.B. (2003b). "Experimental study and calculation of fire resistance of concrete-filled hollow steel columns", *Journal of Structural Engineering*, ASCE, **129**(3), 346-356.
- Klingsch, W. and Wittbecker, F.W. (1988), "Fire resistance of hollow section composite columns of small cross sections", Bergische Universität, Wuppertal, West Germany.
- Kordina, K. and Klingsch, W. (1983), "Fire resistance of composite columns with concrete filled hollow sections", Research report, CIDECT 15 C1/C2 83/27.
- Lie, T.T. and Caron, S.E. (1988), "Fire resistance of circular hollow steel columns filled with siliceous aggregate Concrete", Test results, internal report n°570, Institute for research in Construction, National Research Council of Canada, Ottawa, Canada.

- Lie, T.T. and Caron, S.E. (1988), "Fire resistance of circular hollow steel columns filled with carbonate aggregate Concrete", Test results, Internal report n°573, Institute for research in Construction, National Research Council of Canada, Ottawa, Canada.
- Lie, T.T. and Chabot, M. (1990), "A method to predict the fire resistance of circular concrete filled hollow steel columns", *Journal of Fire Protection Engineering*, **2**(4).
- Lie, T.T. and Chabot, M. (1992), "Experimental studies on the fire resistance of hollow steel columns filled with plain concrete", NRC-CNRC, Internal report 611.
- Lie, T.T. and Chabot, M. (1994), "Fire resistance tests of square hollow steel columns filled with reinforced concrete", Test results, Internal report n°673, Institute for research in Construction, National Research Council of Canada, Ottawa, Canada.
- Lie, T.T., (1994), "Fire resistance of circular steel columns filled with bar-reinforced concrete", *Journal of Structural Engineering*, **120**(4).
- Lie, T.T., and Stringer, D.C. (1994), "Calculation of fire resistance of steel hollow structural steel columns with plain concrete", *Can. J. Civ. Engrg.*, **21**(3), 382-385.
- Lie, T.T. and Irvin, R.J. (1995), "Fire resistance of rectangular steel columns filled with bar-reinforced concrete", *Journal of Structural Engineering*, **121**(5).
- Lie, T.T. and Kodur, V.K.R. (1996), "Fire resistance of steel columns filled with bar-reinforced concrete", *Journal of Structural Engineering*, **122**(1).
- Omeagher, A.J., Bennetts, I.D., Hutchinson, G.L. and Steven, L.K. (1991), "Modelling of concrete filled tubular columns in fire", BHPR/ENG/R/91/031/PS69.
- Quast, U., Hass, R. and Rudoph, K. (1986), "A computer program for the determination of load bearing and deformation behaviour of uniaxial structural elements under fire action", Technical University Braunschweig.
- Renaud, C., Aribert, J.M., Zhao, B. and Grimault, J.P. (2000), "Fire stability of steel-concrete composite columns with allow steel section made in high strength steel", *French Journal of Steel Construction*, n°3, 5-18.
- Renaud, C., Aribert, J.M., and Zhao, B. (2002), "Proposal of a simple calculation model for the fire resistance of concrete filled hollow section columns", *Proceeding of third European Conference on Steel Structures*, **2**, 1355-1366.
- Schleich, J.B. (1987), "Computer assisted analysis of the fire resistance of steel and composite concrete steel structures", CEC Research Report EUR 10828, EN, Luxembourg.
- Twilt, L. and Haar, P.W. (1984), "Analysis of the discrepancy between the french and german calculation methods for the fire resistance of concrete filled steel columns", IBBC-TNO-report n° B-84-480, September.
- Twilt, L. and Haar, P.W. (1985), "The effect of the mechanical properties and the thermal induced stresses on the discrepancy between the french and german calculation methods for the fire resistance of concrete filled steel columns", IBBC-TNO-report n° B-85-93, March.
- Twilt, L. and Haar, P.W. (1985), "The discrepancy between the french and german calculation methods for the fire resistance of concrete filled steel columns: proposition for harmonisation", IBBC-TNO-report n° B-85-426, August.
- Wickstrom, U. and Sterner, E. (1990), "TASEF: fire technology report", Sweedish National Testing and Research.
- Zhao, B. and Aribert, J.M. (1996), "Finite element method for steel-concrete composite frames taking account of slip and large displacements", *European Journal of Finite Element*, **5**(2), 221-249.
- Zhao, B. and Kruppa, J. (1997), "Fire resistance of composite slabs with profiled steel sheet and of composite steel-concrete beams Part 2: composite beams", Final report of European commission Eur 16822 EN on steel Research.